Journal of Solid State Chemistry 183 (2010) 1878–1883

Contents lists available at ScienceDirect

Journal of Solid State Chemistry

journal homepage: www.elsevier.com/locate/jssc

Shape-controlled solvothermal synthesis of bismuth subcarbonate nanomaterials

Gang Cheng [a], Hanmin Yang [b], Kaifeng Rong [a], Zhong Lu [a], Xianglin Yu [a], Rong Chen [a,*]

[a] Key Laboratory for Green Chemical Process of Ministry of Education and School of Chemical Engineering and Pharmacy, Wuhan Institute of Technology, Xiongchu street, Wuhan 430073, PR China

[b] Key Laboratory of Catalysis and Materials Science of the State Ethnic Affairs Commission & Ministry of Education, South-Central University for Nationalities, Wuhan 430074, PR China

ARTICLE INFO

Article history:
Received 26 April 2010
Received in revised form
27 May 2010
Accepted 6 June 2010
Available online 16 June 2010

Keywords:
Nanostructures
Shape-controlled
Bismuth subcarbonate
Solvothermal

ABSTRACT

Much effort has been devoted to the synthesis of novel nanostructured materials because of their unique properties and potential applications. Bismuth subcarbonate ($(BiO)_2CO_3$) is one of commonly used antibacterial agents against *Helicobacter pylori* (*H. pylori*). Different $(BiO)_2CO_3$ nanostructures such as cube-like nanoparticles, nanobars and nanoplates, were fabricated from bismuth nitrate via a simple solvothermal method. The nanostructures were characterized by powder X-ray diffraction (XRD), scanning electron microscope (SEM), transmission electron microscopy (TEM) and high-resolution transmission electron microscopy (HRTEM). It was found that the solvents and precursors have an influence on the morphologies of $(BiO)_2CO_3$ nanostructures. The possible formation mechanism of different $(BiO)_2CO_3$ nanostructures fabricated under different conditions was also discussed.

1. Introduction

Nanostructured materials have attracted enormous interest because of their novel physical and chemical properties, as well as their promising applications in catalysis, solar cells, chemical sensors and biological antibacterial agents and so on [1,2]. It is well known that the properties of nanomaterials with same composition but different morphologies could be significantly different. Shape control has proven to be effective as size control in fine-tuning the properties and functions of nanostructures [3–5]. In some cases, shape control allows one to tailor the properties with greater versatility than can be achieved otherwise [6]. For instance, Song and his co-workers [7] reported that the CuO urchin-like particles exhibited excellent electrochemical performance for lithium-ion batteries, superior to that of the other nanostructures such as hollow cubes, hollow spheres. Hence, the ability to synthesize nanostructured materials with desired shapes is very important in investigating the related fascinating properties and exploring their applications. In the past decade, significant progress in the shape-controlled synthesis of functional nanomaterials has been achieved. Shape-controlled α-Fe_2O_3 [8], $CdCO_3$ [9], Cu [10], CdSe [11], CuS [12], Co_3O_4 [13] and $CoCO_3$ [14] nanostructures were successfully synthesized via various methods. Among these methods, solvothermal synthesis has become an important and promising approach to prepare controlled inorganic nanocrystals [15–17]. It is an ideal technique for synthesizing nanomaterials with high purity, high crystallinity and controlled morphology [15,18].

During the past decade, much effort has been made on the fabrication of bismuth nanostructured materials due to their potential applications in semiconductors, catalysts and biomedicine [19–21]. In recent years, different bismuth nanostructures such as Bi_2WO_6 nanoplates, $BiVO_4$ nanoplates and nanorods, were synthesized by solvothermal method [22,23]. Bismuth subcarbonate ($(BiO)_2CO_3$) is one of the most commonly used antibacterial agents against *Helicobacter pylori* (*H. pylori*), which is Gram-negative bacteria causing peptic ulcers and gastritis [24,25]. In our previous work, bismuth subcarbonate nanotubes were also found to exhibit enhanced antibacterial properties against *H. Pylori* compared with the bulk materials [26]. Recently, there is an increasing interest in the synthesis of different $(BiO)_2CO_3$ nanostructures to develop the treatment of *H. pylori* infection. However, to the best of our knowledge, there are few literatures relevant to the fabrication of different bismuth subcarbonate nanostructures. Up to now, only $(BiO)_2CO_3$ nanotubes [26], nanoparticles [27], irregular sheet-like nanoscale crystals [28] and flower-like hierarchitecture [29] were obtained, which limited its further applications. Therefore, the development of new strategies for the synthesis of novel nanostructured bismuth subcarbonate is highly desired.

In this study, we reported shape-controlled synthesis of bismuth subcarbonate nanostructures by solvothermal method using bismuth nitrate as bismuth precursor. When bismuth

* Corresponding author. Fax: +86 2787194465.
E-mail address: rchenhku@hotmail.com (R. Chen).

0022-4596/$ - see front matter © 2010 Elsevier Inc. All rights reserved.
doi:10.1016/j.jssc.2010.06.004

nitrate was dissolved to different solvents, $(BiO)_2CO_3$ nanomaterials with different shapes such as cube-like nanoparticles and nanoplates were obtained. It was also found that the precursors had an influence on the morphologies of $(BiO)_2CO_3$ nanostructures.

2. Experimental

In a typical experiment, 0.486 g $Bi(NO_3)_3 \cdot 5H_2O$ (1 mmol) was put into 50 mL round-bottom flask which contained 25 mL 0.5 mol/L mannitol solution. The mixture was stirred and sonicated until $Bi(NO_3)_3 \cdot 5H_2O$ was dissolved, followed by addition of 5 mL saturated sodium carbonate solution, resulting in the formation of uniform white suspension. Then the mixture was transferred to a Teflon-lined stainless-steel autoclave to perform solvothermal process at 150 °C for 12 h. After cooled down to the room temperature, the solid product was collected by centrifugation and washed with deionized water for five times. The sample was finally dried in a desiccator for few days at room temperature for further characterization (**BS2**). Other samples were also prepared under identical conditions by changing mannitol concentration, reagents and solvents. The detailed procedure is the same as described above and all the experiment parameters are listed in Table 1.

The $(BiO)_2CO_3$ nanostructures were characterized by powder X-ray diffraction (XRD), scanning electron microscopy (SEM), transmission electron microscopy (TEM) and high-resolution transmission electron microscopy (HRTEM). X-ray diffraction (XRD) was carried on Bruker axs D8 Discover (Cu $K\alpha = 1.5406$ Å). The scanning rate is $1^\circ\ min^{-1}$ in the 2θ range from 10° to 80°. TEM and HRTEM images were recorded on a Philips Tecnai 20 electron microscope, using an accelerating voltage of 200 kV. The SEM images were taken on a LEO 1530 and Hitachi S4800 scanning electron microscope operating at 5 kV. The samples for TEM observations were prepared by dispersing some of the solid products into ethanol and then sonicated for about 30 s. A few drops of the suspension were deposited on the copper grid, which was then put into the desiccator.

3. Results and discussion

The purity and crystallinity of the as-synthesized products (**BS1**, **BS2** and **BS3**) were examined by powder X-ray diffraction (XRD). The XRD patterns of the products prepared by using different mannitol concentrations (**BS1**, **BS2** and **BS3**) were shown in Fig. 1. Each of the diffraction pattern in Fig. 1 can be readily indexed to the tetragonal $(BiO)_2CO_3$ (JCPDS no. 41-1488), indicating the formation of pure $(BiO)_2CO_3$ products. The sharp and strong diffraction peaks also confirm the well crystallization of the products. The strongest diffraction peak corresponds to the (013) crystal plane.

The morphologies and structures of the as-synthesized $(BiO)_2CO_3$ nanomaterials (**BS1**, **BS2** and **BS3**) were further investigated by SEM, TEM and HRTEM as shown in Fig. 2. Fig. 2a gives the representative SEM image of the $(BiO)_2CO_3$ nanostructures obtained in 0.1 M mannitol solution, which suggests that the product consists of a large quantity of uniform cube-like nanoparticles with an average diameter of 45 nm. TEM image shown in Fig. 2b depicts the morphology of the obtained product (**BS1**), indicating the formation of uniform, regular and well-dispersed cube-like nanoparticles. The magnified image (inset of Fig. 2b) further exhibits detailed morphology of this sample. Furthermore, it can be observed that the cube-like nanoparticles are very sensitive to the electronic beam and the edges of the nanoparticles are easily destroyed. More detailed structural information of synthesized products was provided by HRTEM analysis. The lattice fringes could be clearly observed, and the measured *d*-spacing of the crystallographic planes is about 0.689 nm, which is close to the (002) lattice plane of $(BiO)_2CO_3$ crystal. It is suggested that the $(BiO)_2CO_3$ nanoparticles have a high order of crystallinity. However, when the mannitol concentration was increased to 0.5 and 0.9 M, the obtained products presented different morphologies, size distribution and dispersity compared with that of the sample prepared in 0.1 M mannitol solution. Aggregated nanoparticles with irregular morphologies were observed, as depicted in SEM images

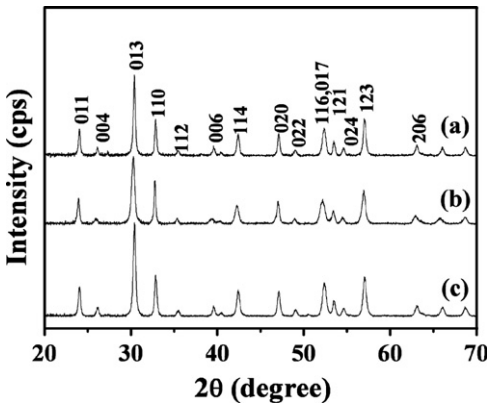

Fig. 1. XRD patterns of the as-synthesized products (**BS1**, **BS2** and **BS3**) prepared from Na_2CO_3 using different mannitol concentrations: (a) 0.1 M, (b) 0.5 M and (c) 0.9 M.

Table 1
Experimental conditions for the synthesis of $(BiO)_2CO_3$ nanostructures.

Sample	Bismuth precursor[a]	Reagent[b]	Solvent[c]	Temperature (°C)	Reaction time (h)
BS1	$Bi(NO_3)_3 \cdot 5H_2O$	Na_2CO_3	0.1 M mannitol	150	12
BS2	$Bi(NO_3)_3 \cdot 5H_2O$	Na_2CO_3	0.5 M mannitol	150	12
BS3	$Bi(NO_3)_3 \cdot 5H_2O$	Na_2CO_3	0.9 M mannitol	150	12
BS4	$Bi(NO_3)_3 \cdot 5H_2O$	$(NH_2)_2CO$	0.1 M mannitol	150	12
BS5	$Bi(NO_3)_3 \cdot 5H_2O$	$(NH_4)_2CO_3$	0.1 M mannitol	150	12
BS6	$Bi(NO_3)_3 \cdot 5H_2O$	Na_2CO_3	0.1 M D-glucitol	150	12
BS7	$Bi(NO_3)_3 \cdot 5H_2O$	Na_2CO_3	Glycerol/distilled water (3:2)	150	12
BS8	$Bi(NO_3)_3 \cdot 5H_2O$	Na_2CO_3	EG	150	12
BS9	$Bi(NO_3)_3 \cdot 5H_2O$	Na_2CO_3	DEG	150	12
BS10	$Bi(NO_3)_3 \cdot 5H_2O$	Na_2CO_3	TEG	150	12

[a] The molar of bismuth precursor was 1 mmol.
[b] The volume of saturated reagent solution was 5 mL.
[c] The volume of solvent was 25 mL.

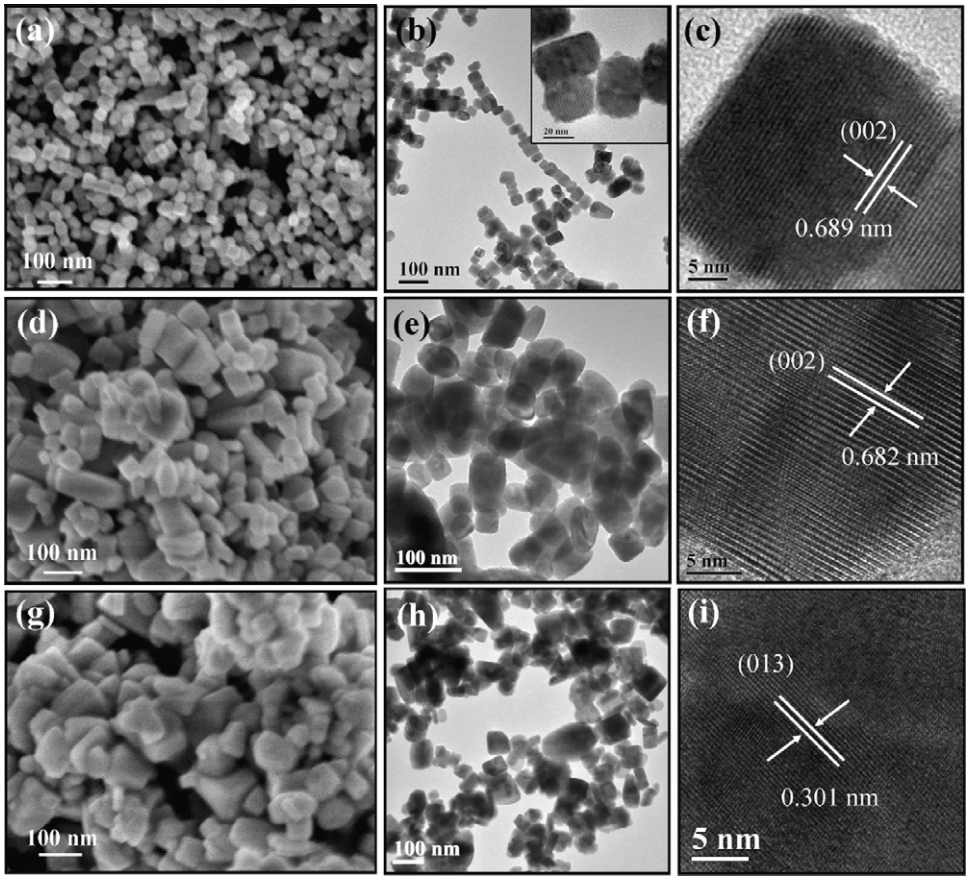

Fig. 2. SEM images (a, d and g), TEM images (b, e and h) and HRTEM images (c, f and i) of $(BiO)_2CO_3$ nanostructures (**BS1**, **BS2** and **BS3**) obtained in mannitol solution with different concentrations: (a–c) 0.1 M, (d–f) 0.5 M and (g–i) 0.9 M.

(Figs. 2d and g). It was found that the sizes of these nanoparticles varied from 20 to 200 nm. TEM images of these two samples (**BS2** and **BS3**) further verified the observations. The nanoparticles showed an obviously aggregation tendency to form irregular large particles with the increase of mannitol concentration (Figs. 2e and h). The corresponding HRTEM images of samples **BS2** and **BS3** were presented in Figs. 2f and i. Lattice fringes can be clearly observed from the HRTEM images, suggesting that the $(BiO)_2CO_3$ nanoparticles are highly crystalline. The lattice plane spacing calculated from the HRTEM images were 0.682 and 0.301 nm, which corresponded to (002) and (013) plane, respectively. The experimental results indicated that the mannitol concentration played a key role in the formation of $(BiO)_2CO_3$ nanocrystals. It was proposed that the viscosity of reaction medium increased with the increase of mannitol concentration, resulting in the aggregation of $(BiO)_2CO_3$ nanomaterials and the increase of the particle sizes.

The influences of experimental parameters on the structure of the final products were investigated systemically. Under identical experimental condition (mannitol concentration is 0.1 M), $(NH_2)_2CO$ and $(NH_4)_2CO_3$ was used as a precursor to synthesize $(BiO)_2CO_3$ nanomaterials, respectively, instead of Na_2CO_3. As shown in Fig. 3, the XRD patterns of samples **BS4** (Fig. 3a) and **BS5** (Fig. 3b) also could be perfectly indexed to tetragonal $(BiO)_2CO_3$ (JCPDS no. 41-1488), indicative of the production of well crystalline pure $(BiO)_2CO_3$ by using $(NH_4)_2CO_3$ or $(NH_2)_2CO$ as reagent. Figs. 3c and d showed the SEM images of samples **BS4** and **BS5**, respectively. When $(NH_2)_2CO$ was used as reagent, a large quantity of polyhedral nanoparticles was obtained. Interestingly, most of products were $(BiO)_2CO_3$ nanobars when $(NH_4)_2CO_3$ was used as precursor. The nanostructures were also examined by TEM and HRTEM images. Figs. 3e–h showed the corresponding TEM and HRTEM images of $(BiO)_2CO_3$ nanostructures prepared by $(NH_4)_2CO_3$ and $(NH_2)_2CO$ (**BS4** and **BS5**). As shown in Fig. 3e, irregular polyhedral nanoparticles were observed and most of them have spherical-like morphologies (inset of Fig. 3g). The lattice plane spacing calculated from the HRTEM images of selected nanoparticles in Fig. 3e was 0.374 nm, which corresponded to (011) plane. Fig. 3f depicts the fabrication of $(BiO)_2CO_3$ nanobars by using $(NH_4)_2CO_3$ as reagent. Inset of Fig. 3h exhibits the more detailed morphology of a selected nanobar. The length of these nanobars varied from 100 to 300 nm and most of them are 200 nm in length. The lattice plane spacing calculated from the HRTEM images of a selected nanobar in Fig. 3f is 0.372 nm, which corresponds to (011) plane.

In order to investigate the effects of solvents on the morphologies of $(BiO)_2CO_3$ nanostructures, D-glucitol, EG, DEG, TEG and glycerol/distilled water mixed-solvent (the volume ratio is 3:2) were used as solvent in the preparation of $(BiO)_2CO_3$ nanostructures (**BS6**–**BS10**). Fig. 4 shows the XRD patterns of the products prepared in different solvents. The diffraction peaks in each pattern are perfectly indexed as tetragonal $(BiO)_2CO_3$ (JCPDS no. 41-1488). No other diffraction peaks were detected from these patterns, indicating the production of high purity $(BiO)_2CO_3$ in the 0.1 M D-glucitol, EG, DEG, TEG and glycerol/distilled water mixed-solvent. The sharp and strong peak also confirmed the products were highly crystalline.

Uniform $(BiO)_2CO_3$ cube-like nanoparticles were also obtained in 0.1 M D-glucitol by solvothermal method (Fig. 5a). The sizes of these nanoparticles are almost 90 nm (Fig. 5b). HRTEM image of a

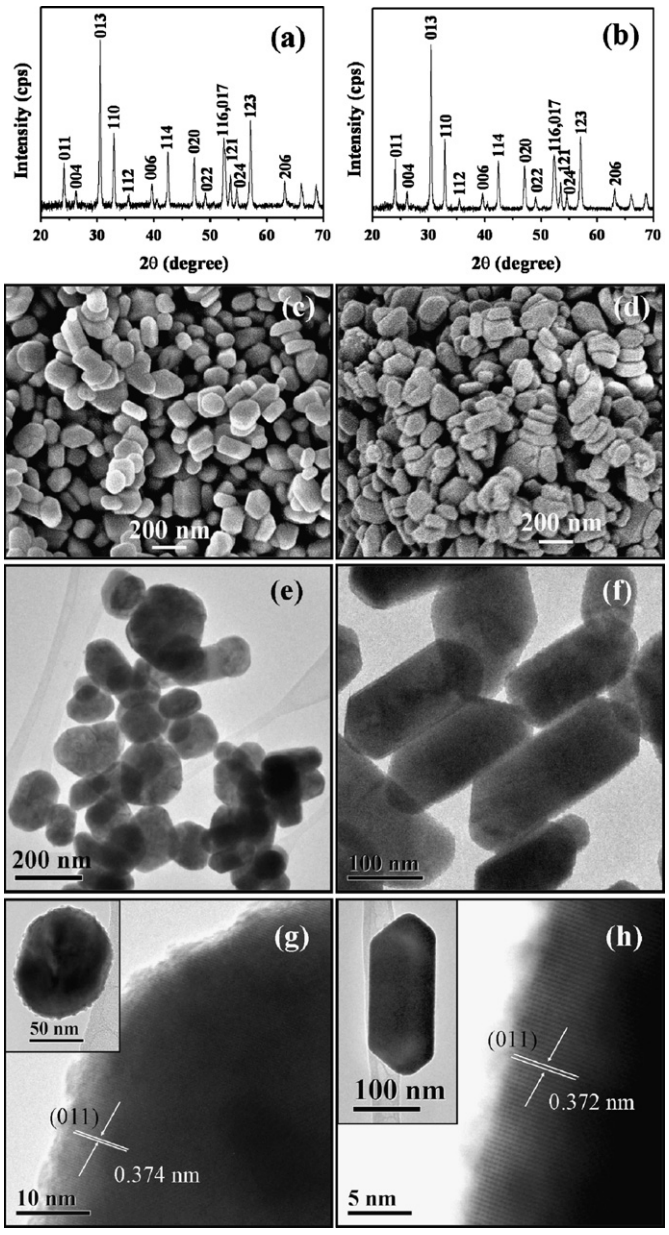

Fig. 3. XRD patterns (a and b) of $(BiO)_2CO_3$ products prepared from $(NH_2)_2CO$ (a: **BS4**) and $(NH_4)_2CO_3$ (b: **BS5**); SEM (c and d), TEM (e and f) and HRTEM (g and h) images of $(BiO)_2CO_3$ nanostructures prepared from $(NH_2)_2CO$ (c, e and g: **BS4**) and $(NH_4)_2CO_3$ (d, f and h: **BS5**).

selected nanoparticle reveals clear lattice fringes with *d*-spacing of 0.683 nm, which corresponds to (002) plane (Fig. 5c). However, only nanoplates were obtained in glycerol/distilled water mixed-solvent, EG, DEG and TEG, as depicted in SEM images (Figs. 5d, g, j and m, respectively). In these solvents, different shaped $(BiO)_2CO_3$ nanoplates were fabricated. The $(BiO)_2CO_3$ nanoplates prepared in glycerol/water solution (**BS7**) have uniform thickness of 60 nm (Figs. 5d and e). When EG was used as solvent, uniform nanoplates with diameter of 100 nm were fabricated, which have a thickness of 40 nm (Figs. 5g and h). However, with the increase of solvent viscosity (TEG > DEG > EG), irregular and unequirotal nanoplates were obtained in the presence of DEG and TEG (Figs. 5j and m). It also can be observed in their TEM images (Figs. 5k and n). Further examination of the crystal structure of the different $(BiO)_2CO_3$ nanoplates were revealed by HRTEM images. Each HRTEM image of a selected nanoplate in

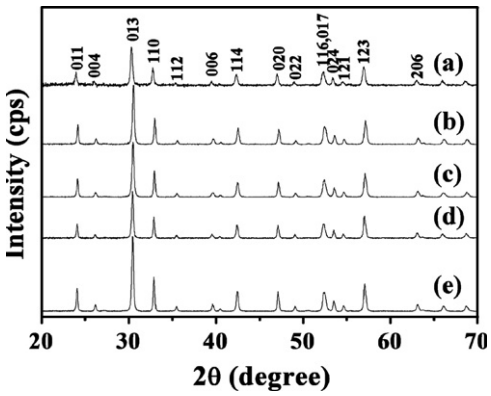

Fig. 4. XRD patterns of the as-synthesized products (**BS6–BS10**) prepared from Na_2CO_3 in different solvents: (a) 0.1 M D-glucitol, (b) glycerol/distilled water mixed-solvent, (c) EG, (d) DEG and (e) TEG.

samples **BS7–BS10** reveals clearly lattice fringes, indicating a single crystal structure of these samples. The lattice *d*-spacing calculated from the HRTEM images is 0.273, 0.275, 0.276 and 0.276 nm, which is very close to the interplanar spacing of (110) plane.

In this synthesis, both the reagents and solvents play a key role in the fabrication of $(BiO)_2CO_3$ nanostructures. It is well known that the formation of specific nanostructures involves two steps: initial nucleation stage and crystal growth stage, which involve a fast nucleation of amorphous primary particles followed by a slow aggregation and crystallization of primary particles [12,30,31]. According to the experimental results, we speculated that the formation of different $(BiO)_2CO_3$ nanostructures was also involved in the nucleation and the subsequent growth process. That is, $(BiO)_2CO_3$ nuclei were formed at the initial stage, followed by the nuclei growth and formation of different $(BiO)_2CO_3$ architectures. We can conclude from the results that different reagents, including sodium carbonate, urea and salvolatile, were also used as structure-directing agents in the solvothermal process, resulting in the fabrication of different shaped $(BiO)_2CO_3$ nanostructures. It is similar with the fabrication of magnetite spheres in the literature [32]. We also proposed that different solvents resulted in different preferential growth of $(BiO)_2CO_3$ nuclei, due to the intrinsic anisotropic characteristics of the $(BiO)_2CO_3$ tetragonal crystal structure. It was reported that bismuth salts can form Bi^{III}-glycerol complexes and Bi^{III}-EG complexes in glycerol and EG, respectively [33–35]. In this synthesis, it was proposed that the possible bismuth complexes (Bi^{III}-mannitol, Bi^{III}-glucitol, Bi^{III}-glycerol, Bi^{III}-EG, Bi^{III}-DEG and Bi^{III}-TEG complexes) were formed in different solvents before the solvothermal process. Under the solvothermal condition, bismuth complexes reacted with Na_2CO_3 to form $(BiO)_2CO_3$ nuclei, then grew into different shaped $(BiO)_2CO_3$ nanocrystals under the directing of different solvents through Ostwald ripening process [36,37]. The results indicate that the morphologies and dispersity of $(BiO)_2CO_3$ nanostructures can be controlled by the number of hydroxyl groups on the solvent and the solution viscosity. The solvents used have six hydroxyl groups (mannitol and glucitol), three hydroxyl groups (glycerol) or two hydroxyl groups (EG, DEG and TEG, respectively). Uniform cube-like nanoparticles were fabricated in mannitol with six hydroxyl groups. D-glucitol is the isomer of mannitol, which also resulted in the formation of cube-like $(BiO)_2CO_3$ nanoparticles. In other solvents which contained two or three hydroxyl groups, $(BiO)_2CO_3$ nanoplates were obtained. It may arises from the different ability of multiple hydroxyl groups to bind to the nanocrystals as they grow. Tilley and his coworkers [38] also reported the influence of number of

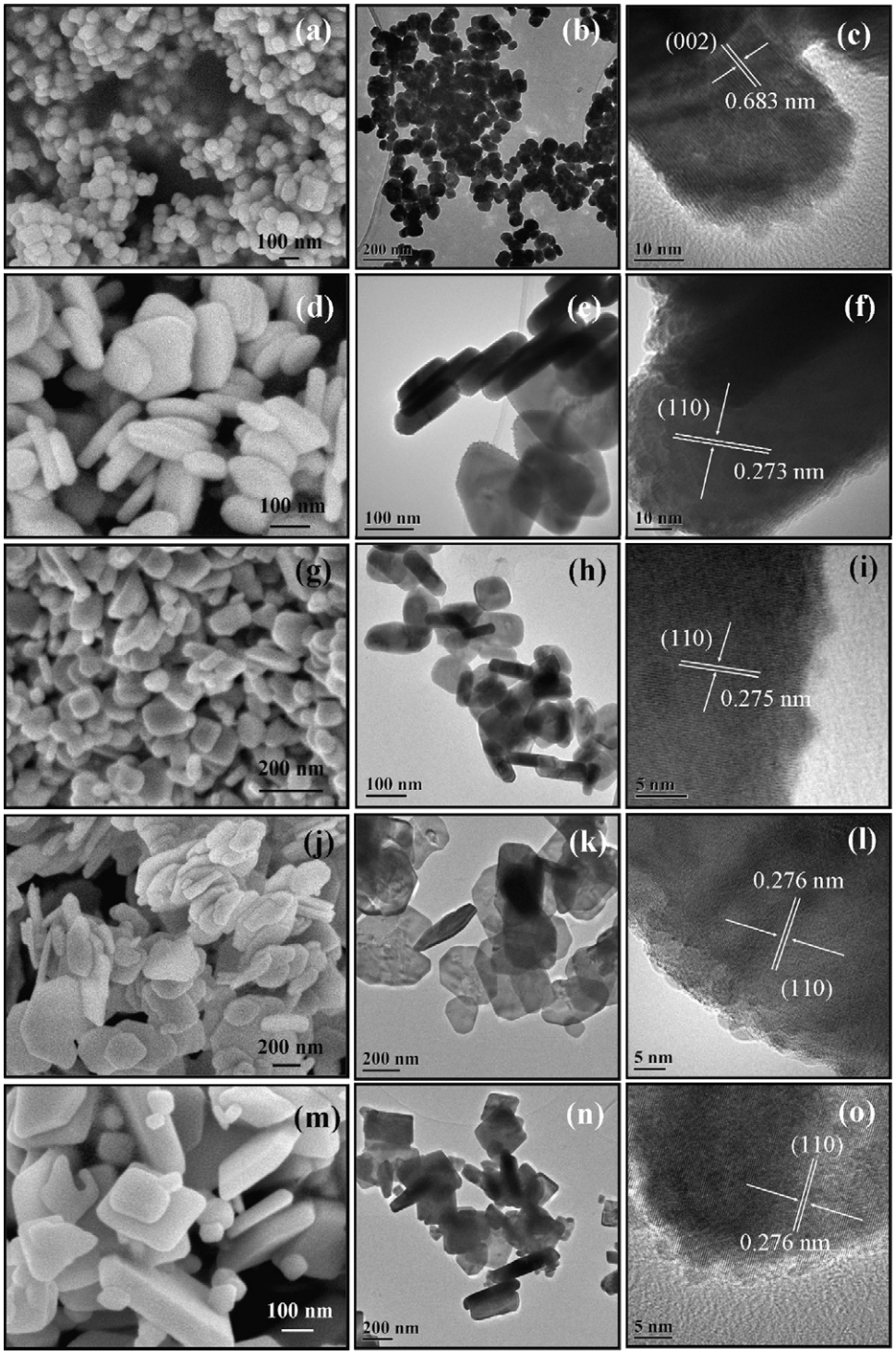

Fig. 5. SEM image (a, d, g, j and m) TEM image (b, e, h, k and n) and HRTEM image (c, f, i, l and o) of $(BiO)_2CO_3$ nanostructures (**BS6–BS10**) prepared from Na_2CO_3 in different solvents: (a–c) 0.1 M D-glucitol, (d–f) glycerol/distilled water mixed-solvent, (g–i) EG, (j–l) DEG and (m–o) TEG.

hydroxyl groups on the synthesis of SnS quantum dot. At the same time, the viscosity of the solvent also influences the dispersity of the nanostructures. Low viscosity in 0.1 M mannitol or D-glucitol favors the formation of well-separated cube-like $(BiO)_2CO_3$ nanoparticles. With the increase of viscosity (TEG > DEG > EG > -glycerol/water), the slow diffusion occurs, leading to the formation of irregular $(BiO)_2CO_3$ nanoplates with poor dispersity. Our understanding of the formation mechanism is limited and further investigation is still in progress.

4. Conclusion

In summary, different bismuth subcarbonate nanostructures, such as cube-like nanoparticles, nanobars and nanoplates were synthesized via a simple solvothermal process. It was found that both solvent and reagent have a significant influence on the morphologies and dispersity of the $(BiO)_2CO_3$ nanostructures. The possible formation mechanism of different $(BiO)_2CO_3$ nanostructures prepared under different conditions was also discussed.

It provides a facile route to synthesize different shaped $(BiO)_2CO_3$ nanostructures for the further investigation of their antibacterial properties against *H. pylori*. In addition, these nanostructures can serve as a template or bismuth precursor to prepare Bi_2E_3 (E=S, Se, Te, etc.) and other bismuth-contained nanocrystals. The convenient technique might also be extended to synthesize other bismuth nanomaterials such as bismuth oxyhalide (BiOX, X=Cl, Br, I).

Acknowledgments

This work was supported by the National Natural Science Foundation of China (Grant 20801043), the Program for New Century Excellent Talents in University (NCET-09-0136), Wuhan Chenguang Scheme (Grant 200850731376) established under Wuhan Science and Technology Bureau and the Open Research Fund of Key Laboratory of Catalysis and Materials Science of the State Ethnic Affairs Commission & Ministry of Education (No. CHCL09010). We thank Mr. Frankie Y.F. Chan (The University of Hong Kong) for his kind help with TEM characterizations.

References

[1] T. Rueckes, K. Kim, E. Joselevich, G.Y. Tseng, C.L. Cheung, C.M. Lieber, Science 289 (2000) 94–97.
[2] Y. Cui, C.M. Lieber, Science 291 (2001) 851–853.
[3] C. Burda, X. Chen, R. Narayanan, M.A. El-Sayed, Chem. Rev. 105 (2005) 1025–1102.
[4] F. Gao, Q. Lu, S. Komarneni, Chem. Mater. 17 (2005) 856–860.
[5] Y. Xia, P. Yang, Y. Sun, Y. Wu, B. Mayers, B. Gates, Y. Yin, F. Kim, H. Yan, Adv. Mater. 15 (2003) 353–389.
[6] Y. Xiong, Y. Xia, Adv. Mater. 19 (2007) 3385–3391.
[7] J.C. Park, J. Kim, H. Kwon, H. Song, Adv. Mater. 21 (2009) 803–807.
[8] G.H. Wang, W.C. Li, K.M. Jia, B. Spliethoff, F. Schuth, A.H. Lu, Appl. Catal. A: Gen. 364 (2009) 42–47.
[9] Z. Jia, Y. Tang, L. Luo, B. Li, Cryst. Growth Des. 8 (2008) 2116–2120.
[10] D. Mott, J. Galkowski, L. Wang, J. Luo, C.J. Zhong, Langmuir 23 (2007) 5740–5745.
[11] L.S. Li, J.T. Hu, W.D. Yang, A.P. Alivisatos, Nano Lett. 1 (2001) 349–351.
[12] W. Du, X. Qian, X. Ma, Q. Gong, H. Cao, J. Yin, Chem. Eur. J. 13 (2007) 3241–3247.
[13] Y. Dong, K. He, L. Yin, A. Zhang, Nanotechnology 18 (2007) 435602/1–435602/6.
[14] H.P. Cong, S.H. Yu, Cryst. Growth Des. 9 (2009) 210–217.
[15] X. Wang, J. Zhuang, Q. Peng, Y. Li, Nature 437 (2005) 121–124.
[16] S. Komarneni, M.Z. Hussein, C. Liu, E. Breval, P.B. Malla, Eur. J. Solid State Inorg. Chem. 32 (1995) 837–849.
[17] B.L. Newalkar, S. Komarneni, H. Katsuki, Chem. Commun. (2000) 2389–2390.
[18] R.Q. Song, A.W. Xu, S.H. Yu, J. Am. Chem. Soc. 129 (2007) 4152–4153.
[19] R. Chen, M.H. So, C.M. Che, H. Sun, J. Mater. Chem. 15 (2005) 4540–4545.
[20] M.G. Francesconi, A.L. Kirbyshire, C. Greaves, O. Richard, G. Van Tendeloo, Chem. Mater. 10 (1998) 626–632.
[21] R.C. Oliveira, L.S. Cavalcante, J.C. Sczancoski, E.C. Aguiar, J.W.M. Espinosa, J.A. Varela, P.S. Pizani, E. Longo, J. Alloys Compd. 478 (2009) 661–670.
[22] C. Zhang, Y. Zhu, Chem. Mater. 17 (2005) 3537–3545.
[23] G. Xi, J. Ye, Chem. Commun 46 (2010) 1893–1895.
[24] P.J. Sadler, H. Li, H. Sun, Coord. Chem. Rev. 185–186 (1999) 689–709.
[25] G.B. Glen, B. Neil, Chem. Rev. 99 (1999) 2601–2657.
[26] R. Chen, M.H. So, J. Yang, F. Deng, C.-M. Che, H. Sun, Chem. Commun. (2006) 2265–2267.
[27] R. Chen, G. Cheng, M.H. So, J. Wu, Zhong Lu, C.M. Che, H. Sun, Mater. Res. Bull. 52 (2010) 654–658.
[28] X.Y. Chen, H.S. Huh, S.W. Lee, J. Solid State Chem. 180 (2007) 2510–2516.
[29] Y. Zheng, F. Duan, M. Chen, Y. Xie, J. Mol. Catal. A: Chem. 317 (2010) 34–40.
[30] L. Shi, K. Bao, J. Cao, Y. Qian, Appl. Phys. Lett. 93 (2008) 152511/1–152511/3.
[31] Y. Li, M.H. Cao, L.Y. Feng, Langmuir 25 (2009) 1705–1712.
[32] D.P. Singh, A.K. Ojha, O.N. Srivastava, J. Phys. Chem. C 113 (2009) 900–906.
[33] Z.P. Liu, S. Peng, Q. Xie, Z.K. Hu, Y. Yang, S.Y. Zhang, Y.T. Qian, Adv. Mater. 15 (2003) 936–940.
[34] Y.H. Gao, H.L. Niu, C. Zeng, Q.W. Chen, Chem. Phys. Lett. 367 (2003) 141–144.
[35] Z.P. Liu, J.B. Liang, S. Li, S. Peng, Y.T. Qian, Chem. Eur. J. 10 (2004) 634–640.
[36] Y. Chang, J.J. Teo, H.C. Zeng, Langmuir 21 (2005) 1074–1079.
[37] R. Qiao, X.L. Zhang, R. Qiu, J.C. Kim, Y.S. Kang, Chem. Mater. 19 (2007) 6485–6491.
[38] Y. Xu, N. Al-Salim, C.W. Bumby, R.D. Tilley, J. Am. Chem. Soc. 131 (2009) 15990–15991.